MATTER: International Journal of Science and Technology
ISSN 2454-5880

Pfennig et al., 2019

Volume 5 Issue 1, pp. 115-137

Date of Publication: 16th April 2019

DOI-https://dx.doi.org/10.20319/mijst.2019.51.115137

This paper can be cited as: Pfennig, A., Gröber, A., Simkin, R., & Kranzmann, A. (2019). Influence of Surface Quality on the Corrosion and Corrosion Fatigue Behavior of High Alloyed Steels Exposed to Different Saline Aquifer Water Environments. MATTER: International Journal of Science and Technology, 5(1), 115-137.

INFLUENCE OF SURFACE QUALITY ON THE CORROSION AND CORROSION FATIGUE BEHAVIOR OF HIGH ALLOYED STEELS EXPOSED TO DIFFERENT SALINE AQUIFER WATER ENVIRONMENTS

Anja Pfennig
HTW-Berlin, University of Applied Sciences, Berlin, Germany
anja.pfennig@htw-berlin.de

Andre Gröber
HTW-Berlin, University of Applied Sciences, Berlin, Germany

Roman Simkin
BAM, Federal Institute for Materials Research and Testing Berlin, Berlin, Germany
roman.simkin@bam.de

Axel Kranzmann
BAM, Federal Institute for Materials Research and Testing Berlin, Berlin, Germany
axel.kranzmann@bam.de

Abstract

Coupons of X5CrNiCuNb16-4 with different surface roughness that may be utilized as injection pipe with 16% Chromium and 0.05% Carbon (1.4542, AISI 630) were exposed for 3000 h to CO_2-saturated saline aquifer water simulating the conditions in the Northern German Basin at ambient pressure and 60 °C. Additionally, corrosion fatigue experiments (ambient pressure, technically clean CO2, saline aquifer water of Stuttgart Aquifer) were performed using specimen of X46Cr13 (1.4043, AISI 420C) with regard to the influence of the roughness of technical

surfaces on the number of cycles to failure at different stress amplitudes. Specimen of duplex stainless steel X2CrNiMoN22-3-2 (1.4462) for corrosion fatigue experiments were provided with technical surfaces after machining as well as polished surfaces. Results were obtained at load amplitudes ranging from 175 MPa to 325 MPa in the geothermal brine of the Northern German Basin at 98 °C. The main precipitation phases on the surface as well as within pits reveal carbonates or hydroxides such as siderite ($FeCO_3$) and ferrous hydroxide goethite (FeOOH) independent of the original surface roughness. Corrosion rates for polished and technical surfaces were below 0.005 mm/year compared to corrosion rates of 0.035 mm/year after shot peening. Specimen with technical surfaces tested at high stress amplitudes (>275 MPa) lasted longer (cycles to failure: P50% at S_a 300 MPa=$5x10^5$) than specimen with polished surfaces (cycles to failure: P50% at S_a 300 MPa=$1.5x10^5$). This behavior is emphasized by the slope coefficient (technical surfaces k = 19.006, polished surfaces k=8.78) meaning earlier failure for polished at high stress amplitude S_a. Although rather low scatter ranges (technical surface: TN=1:1.35, polished surface: TN=1.1.95) indicate no change in failure mechanism it may be assumed that at low stress pitting is the initiating crack growth process whereas at high stress amplitudes the formation of micro cracks is reason for crack propagation and failure.

Keywords

High Alloyed Steel, Pitting, Surface, Roughness, Corrosion Fatigue, Corrosion, CCS, CO_2-Storage

1. Introduction

CCS known as Carbon Capture and Storage is discussed to mitigate global warming by reducing the emission of the greenhouse gas CO_2 emitted mainly from power plants. The CCS procedure includes first the capture of CO_2 from the emitting source, second the transport through pipelines and third the injection into appropriate geological formations (Thomas, 2005; Ruhl, Göbel Kranzmann, 2012; Gale, 2004). During the injection of CO_2 into deep geological saline aquifer reservoirs as found in the Northern German Basin (Förster et al., 2006; Förster et al., 2010; Kissinger et al., 2014; Wei, Pang, Liu, Gao, 2015; Nešić, 2007), the CO_2 is dissolved in the aquifer water building a highly corrosive environment easily causing the failure of pipe steels (Wei, Pang, Liu, Gao, 2015; Carvalho, Joia, Mattos, 2005). A $FeCO_3$ corrosion layer (siderite) precipitates on the surface because of the iron dissolution of the pipe steel (Wei, Pang, Liu, Gao, 2015; Cui, Wu, Zhu, Yang, 2006). In CO_2-rich environment simultaneous anodic and

cathodic reactions will form corrosion products that precipitate on the surface of the steel (Pfennig and Kranzmann, 2011). Main components are: $FeCO_3$ (siderite), $Fe(HCO_3)_2$ (iron bi-carbonate) and FeOOH (goethite) (Wei, Pang, Liu, Gao, 2015; Pfennig and Kranzmann, 2011)

All corrosion processes in CCS environment are reliant upon the source of the injected gas, its composition as well as the presence of water and dissolved salts (Wei, Pang, Liu, Gao, 2015; Carvalho, Joia, Mattos, 2005). While the corrosion resistance of high alloyed steel is fairly good the injection pipe in CO_2-rich aquifer water may corrode if phase boundaries will form during possible backflow of the aquifer water into the injection pipe when the injection process is intermitted (Pfennig, Kranzmann, 2011; Wu et al., 2004; Akbari Mousavi, Sufizadeh, 2009).

1.4043 is a well-known martensitic stainless (13% Cr, 0.46% C) that is widely used in industry. Precipitation hardening martensitic stainless steel (1.4542, AISI 630, X5CrNiCuNb16-4) containes approximately 3% small size copper to trigger the precipitation hardening mechanism (Islam, Sun, 2016). Niobium and copper carbides are locally embedded within the layered microstructure of 1.4542 consisting of a bcc martensitic matrix (Wang, Zou, 2006) to increase the strength of the steel and ensure excellent mechanical properties along with good corrosion resistance. However, the high strength martensitic state of the microstructure corrodes more easily than the low strength solution treated state. Duplex stainless steel (DSS) X2 CrNiMoN 22 5 3 (1.4462, UNS S31803) provides excellent general corrosion resistance (Schultze et al., 2001; Arnold, Gümpel, Heitz, 1999) and good resistance to stress corrosion cracking SCC (Prosek et al., 2014). The corrosion and corrosion fatigue behaviour has been reported earlier (Pfennig et al., 2014; Vollmar, Roeder, 1994; Lo and Tsai, 2007; Mathis, 1987), but not for CCS or geothermal environments.

1.1.Influence on Static Behavior

Different authors show a direct dependence of the mechanical and corrosion behavior of various steel qualities on the surface roughness resulting from machining processes (Zhang et al., 2016; Takemoto, 1984; Nor Asma, Yuli, Mokhtar, 2010; Maranhão and Davim, 2010; Martin et al., 2011; Evgenya, Hughesa, Eskinba, 2016; Xu et al., 2016; Llaneza, Belzunce, 2015; Lee, Lee, Kim, Jang, 2012; Lv, Guo, Liang, 2016; Ahmed et al., 2015; Shaharyari, Kamal, Omanovic, 2008). In general, the corrosion resistance increases with decreasing valley of depth on the surface for carbon steel (Evgenya, Hughesa, Eskinba, 2016; Xu et al., 2016), austenitic stainless steel (Zhanga et al., 2016; Shaharyari, Kamal, Omanovic, 2008) after shot peeing (Ahmed et al., 2015) and ferritic stainless steel when R_a exceeded 0.5 µm (Lee, Lee, Kim, Jang, 2012).

For 316L austenitic stainless steel Zhang et al., 2016 show that the machined surface is highly susceptible to SCC initiation due to a high level of tensile residual stress. The cracking direction is perpendicular to the machining marks because of tensile residual stresses according to the standardized stress corrosion test method ASTM G36. Crack number and density increased significantly for the residual stress surpassing 190 MPa=76% of the yield strength (Takemoto, 1984). On the other hand electro polished surfaces show little cracking where the machined surface layer is removed leaving residual compressive stress in the specimen (Nor Asma, Yuli, Mokhtar, 2010). Pitting corrosion resistance of 2205 DSS decreased in borate buffer solution with chloride ions with the increasing strain (Lv, Guo, Liang, 2016; Ahmed et al., 2015).

Evgeny et al. found that turbulent flow conditions as well as a rough surface of low carbon steels negatively impact the growth rate of an inhibitor film (Evgenya, Hughesa, Eskinba, 2016). Additionally, the corrosion rate is proportional to the surface roughness (R_a) for laminar and turbulent flow conditions increasing with surface roughness. However, Xu et al., 2016 state that the effect of relative humidity outweighs the influence of the initial surface roughness of X70 pipe steels (Xu et al., 2016). A relative humidity of <55% and >88% suppresses the influence of surface roughness on the corrosion rate, but between 60% and 75%, a rougher surface leads to a high corrosion rate (0.8 mm/y) (Xu et al., 2016).

1.2. Influence on Fatigue Behaviour

Many authors correlate smooth surfaces and compressive surface stress with enhanced fatigue behavior in air (Engelmohr and Fiedler, 1991; Kleemann and Zenner, 2006), but also with corrosion resistance resulting in enhanced corrosion fatigue behavior (Sanjurjo et al., 2010); Abdulstaar, Mhaede, Wollmann, Wagner, 2014; Wu et al., 2006). Sanjurjo et al., 2010 state that the elimination of surface stress in combination with improved surface roughness of AISI 2205 stainless duplex steel improved the fatigue behavior by 90% whereas only 10% account for compressive residual stress induced by shot peening. Residual stress was correlated anti-proportional to the corrosion resistance. For AA5083 the corrosion resistance increased after shot peeing and ball burnishing (Abdulstaar, Mhaede, Wollmann, Wagner, 2014). Smooth surfaces and deeper plastic deformations resulted in good fatigue performance under corrosive environment. The degradation of fatigue resistance for ASTM A533B appears at fast strain rates and rougher surface finish in high temperature water (Wu et al, 2006).

In general, the influence on environmental factors (composition of corrosive media and alloy, flow conditions, temperature, CO_2 partial pressure, contaminations and formation of

protective scales have been reported by various authors (Cui, Wu, Zhu, Yang, 2006; Banaš, Lelek-Borkowska, Mazurkiewsicz, Solarksi, 2007; Moreira et al., 2004). Moreover, 60 °C is a critical temperature regime for accelerated corrosion processes (Seiersten, 2001, Carvalho, Joia, Mattos, 2005; Pfennig and Kranzmann, 2014; Wu et al. 2014; Seiersten, 2001; Choi, Y.-S. and Nešić, S., 2008; Han, Zhang, Carey., 2011, Pfennig and Kranzmann, 2012; Pfennig, Linke, Kranzmann, 2011; Mu, Zhao, 2010; Pfennig, Wolthusen, Wolf, Kranzmann, 2014). This study introduces the dependence on the surface treatment of 1.4542 prior to exposure to an artificial brine and simulated CCS conditions (Parts of this work have been presented at GHGT14 in Melbourne, 2018.) Also the dependence of the corrosion fatigue behavior and endurance limit of 1.4462 and 1.4043 on the surface treatment was investigated in geothermal environment at 100 °C.

2. Experimental Set Up

Static corrosion experiments were conducted with 1.4542 (X5CrNiCuNb16-4, AISI 630) (Table 1) (3 mm thickness and 25 mm diameter) heat treated and analyzed according to earlier work (Pfennig, Wolthusen, Wolf, Kranzmann, 2014; Pfennig, Wolthusen, Kranzmann, 2017; Pfennig and Kranzmann, 2012; Pfennig, Linke, Kranzmann, 2011, Pfennig and Kranzmann, 2011).

Table 1: *Element Content of 1.4542 (X5CrNiCuNb16-4, AISI 630), (Mass Percent)*

Element	C	Si	Mn	P	S	Cr	Mo	Ni	Cu	Nb
acc standard [a]	≤ 0.07	≤ 0.70	≤ 1.50	≤ 0.04	≤ 0.015	15.0 - 17.0	≤ 0.60	3.00 – 5.00	3.00 – 5.00	0.20 – 0.45
analysed [b]	0.03	0.42	0.68	0.018	0.002	15.75	0.11	4.54	3.00	0.242

a) elements as specified according to **DIN EN 10088-3 in %** Electron Probe Microanalyzer JXA8900-RLn
b) spark emission spectrometry SPEKTROLAB M

Dynamic corrosion tests (fatigue) used high alloyed steel 1.4043 (X46Cr13, AISI 420C) (Table 2) and duplex steel 1.4462 (X2 CrNiMoN 22 5 3, AISI A182 F51 (329LN)) (Table 3) (Pfennig et al., 2017).

Table 2: *Element Content of 1.4043 (X46Cr13, AISI 420C), (Mass Percent)*

Element	C	Si	Mn	P	S	Cr	Mo	Ni	Co	Fe
acc standard[a]	0.42-0.5	<1.00	≤ 1.00	≤ 0.045	≤ 0.03	12.5 – 14.5				0.20 – 0.45

analysed[b]	0.46	0.25	0.45	0.018	0.003	13,39	0.03	0.13	0.03	85.4

c) elements as specified according to **DIN EN 10088-3 in %** Electron Probe Microanalyzer JXA8900-RLn
d) spark emission spectrometry SPEKTROLAB M

Table 3: *Element Content of 1.4462 X2 CrNiMoN 22 5 3 (UNS S31803) (tmass percent)*

phases	C	Si	Mn	P	S	Cr	Mo	Ni	N
α & γ**	0.023	0.48	1.83	0.024	0.008	22.53	2.92	5.64	0.146
α*	0.02	0.55	1.59	-	-	24.31	3.62	3.81	0.07
γ*	0.03	0.47	1.99	-	-	20.69	2.17	6.54	0.28

Table 4 shows the major mechanical properties and PRE number of both alloys. The PRE-number is calculated by the following equation (1) (Grümpel et al., 2008):

$$PREN = \%Cr + 3.3\% Mo + 16\% N \quad (1)$$

The high strength of 1.4542 primarily from the martensitic microstructure and alloying elements such as Cr, Ni and Cu is accompanied by fabrication process, microstructure and additional alloying elements, in particular nitrogen and (Alvarez-Armas, 2008; Foct, Akdut, 1993). Figure 1 depicts the alloy's microstructure (martensite with different needle shaped sizes and a small percentage of precipitation obtained via etching prior to exposure and fatigue testing. Due to its percentage of austenite 1.4462 reveals a much better corrosion resistance resulting in a PREN number twice as high as 1.4542.

Table 4: *Mechanical Properties of X2 CrNiMoN 22-5-3; tested in Lateral Phase Direction*

Alloy	yield strength (MPa)	tensile strength (MPa)	PREN
X2CrNiMoN22-5-3 Endurance limit in air: 485 MPa	672	854 in air	30.8 – 38.07
X5CrNiCuNb16-4	720	1078 in air	15.0-18.9

2.1 Exposure Tests at Ambient Pressure

The different textures of the surfaces of 1.4542 were activated by

1. Turning,
2. Sand Blasting (Sand 0,1 mm diameter),
3. Sand Blasting (Sand 0,5 mm diameter) and
4. Grinding with SiC-Paper from 180 µm to 1200 µm under water and then finishing with diamond paste 6 µm, 3 µm and 1 µm.

and then positioned within the liquid phase of the laboratory brine similar to the Stuttgart Aquifer (Förster et al, 2006) (Table 5).

Table 5: *Chemical Composition of the Norther German Basin and Stuttgart Formation electrolyte (Förster et al, 2006; Förster et al., 2010)*

According to Northern German Basin (Förster et al., 2010)										
	NaCl	KCl	$CaCl_2$ x $2H_2O$	$MgCl_2$ x $6H_2O$	NH_4Cl	$ZnCl_2$	$SrCl^{2+}$ 6H2O	$PbCl_2$	Na_2SO_4	pH value
g/L	98.22	5.93	207.24	4.18	0.59	0.33	4.72	0.30	0.07	5.4 - 6
According to Stuttgart Formation (Förster et al, 2006)										
	NaCl	KCl	$CaCl_2$ x $2H_2O$	$MgCl_2$ x $6H_2O$	Na_2SO_4 x $10H_2O$	KOH	$NaHCO_3$			pH value
g/L	224.6	0.3902	6.452	10.62	12.074	0.3206	0.0475			8.2 - 9

or

	Ca^{+}	K^{2+}	Mg^{2+}	Na^{2+}	Cl^{-}	SO_4^{2-}	HCO_3^{-}			pH value
g/L	1.76	0.43	1.27	90.1	14.33	3.6	0.04			8.2 - 9

The exposure of the samples was disposed for 1000 h and 3000 h in a chamber kiln at 60 °C and ambient pressure. Flow control of technically clean CO_2 (3 NL/h) was done by a capillary meter GDX600_man by QCAL Messtechnik GmbH, München (Pfennig and Kranzmann, 2011 Pfennig et al., 2011).

2.2 Corrosion Fatigue Tests

The specimen shape and dimensions in accordance to DIN EN ISO 11782 1 and FKM Research Issue (Buschermöhle, 1996) as well as the corrosion chamber set up (Figure 1) was widely described earlier (Beuth Verlag, 2009; Pfennig Wolf, Gröber, Böllinghaus, Kranzmann, 2016; (Bäßler, Sobetzki, Klapper, 2013; Wolf et al., 2006; Pfennig, Heynert, Wolf, Böllinghaus, 2014).

The precision turning of the surfaces was set to Rz=4, polishing routine was SiC-Paper from 180 µm to 1200 µm under water and finish with diamond paste 6 µm, 3 µm and 1 µm. The verification of the surface roughness was accomplished via optical surface scanner FRT MicroProf 300 prior to corrosion fatigue experiments. The surface roughness was examined within the critical cross-section of the specimen. The scanner was operated in the 2D measuring mode, with the measurement length of 3 mm and an interval of 2.1 µm between the measuring points. The surface roughness of the specimens varied from 2.6 µm to 4.7 µm for 1.4542 and 2.4 µm to 5.3 µm for 1.4462, resulting in a mean arithmetic value of 3.65 (1.4542) and 3.2 µm

(1.4462). Surface roughnesses of polished specimens varied from 0.58 µm to 2.01 µm with a mean of 1.59 µm.

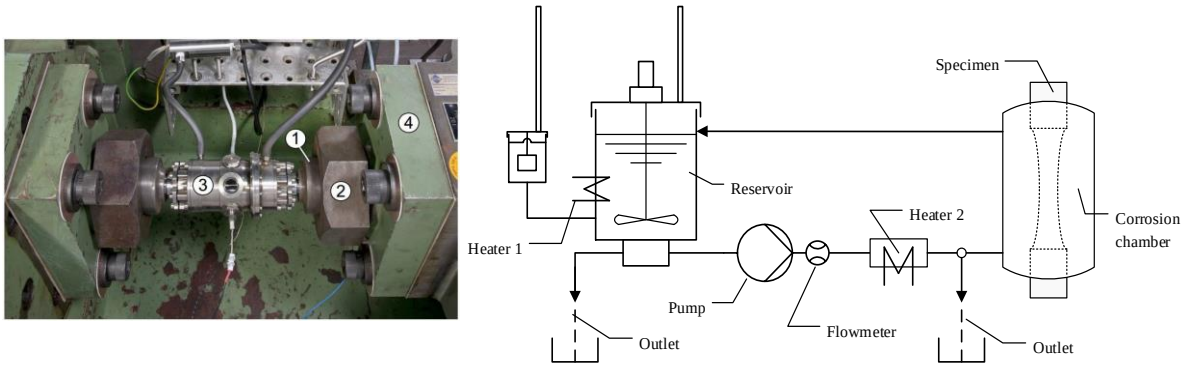

Figure 1: I*n-situ Corrosion Fatigue Testing (Shaharyari et al., 2008; Wolf et al., 2016)*

The corrosion fatigue strength of the high alloyed steel 1.4542 is tested at 60 °C in Stuttgart Aquifer and flowing technically clean CO_2 (99.999%) (Table 5). Duplex steel 1.4462 was examined in dynamic stress-strain tests at 98 °C under CCS conditions according to synthetic Northern German Basin without flowing CO_2 (Wolf et al., 2006; Pfennig, Heynert, Wolf, Böllinghaus, 2014). Therefore a resonant testing machine (sinusoidal dynamic test loads, R=-1; resonant frequency ~ 30 Hz) has been used to test 9 specimens between 280 MPa and 390 MPa.

3. Results and Discussion

The low pressure in the injection pipe during injection intermissions may cause a rising water level into the injection pipe. Consequently a corrosion layer and pits form comprising of siderite $FeCO_3$ and goethite α-FeOOH (Pfennig et al., 2017; Pfennig et al., 2014; Nešić, 2007; Moreira et al., 2004).

3.1 Influence of Surface Condition on Static Corrosion Behavior (X5CrNiCuNb16-4)

Figure 5 states a discontinuous layer structure on sample surfaces when exposed to CO_2-saturated geothermal water. Pit corrosion starts after 1000 h of exposure. Sand blasting the base metal surfaces leads to severe corrosive attack indicated by a surface layer and additional pits. Grinding and polishing lead only to single pits unevenly distributed on the sample surfaces. This dependence on treating the surface prior to exposure is independent of exposure time. The phenomena appear clearly after 1000 h as well as after 3000 h of exposure. However, lower

surface roughness does not results in higher corrosion resistance – technical surfaces reveal high surface roughness but lower corrosion rates than sand blasted surfaces.

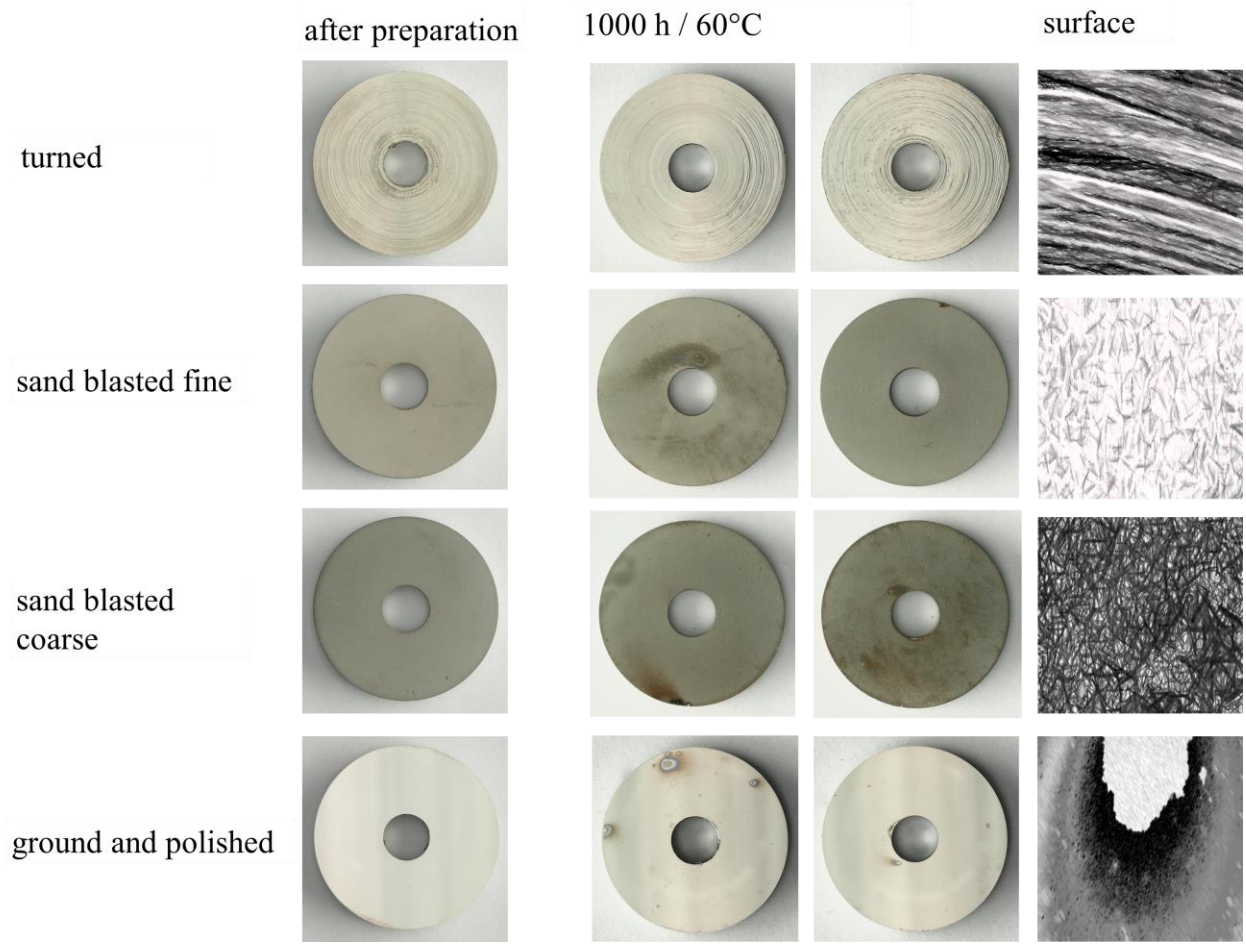

Figure 2: *Sample surfaces of heat treated martensitic stainless steel X5CrNiCuNb16-4 after 1000 h of exposure to and CO_2 saturated saline aquifer water at 60 °C and ambient pressure*

Generally for all samples the corrosion rates are low. Longer exposure increases the corrosion rate for all samples indicating a non-passivating corrosion scale accounting for mutual diffusion of ions towards the metal-aquifer boundary. This is due to the break-down of the initial passivating layer on the high alloyed steel where newly exposed metal surface is susceptible to corrosion scale precipitation and the deterioration of the base metal. Maximum corrosion rate is approximately 0.046 mm/year, after 3000 h for coupons with shot peened surfaces and approximately 0.005 mm/year for technical surfaces and 0.01 mm/year for polished surfaces (Figure 3). The explicit increasing corrosion rates after long exposure to the CO_2-saturated saline aquifer environment may be due to aging accompanied by consolidation and precipitation of carbides besides the passivating layer break-down (Pfennig et al., 2017). The low scatter range of

corrosion rates for polished and technical surfaces (corrosion rate=0.004 mm/year) and the high scatter range of sand blasted samples (corrosion rate=0.02 mm/year) is most likely due to the local differences in surface roughness and increased surface area resulting from the sand blasting process promoting different rates of the corrosive attack.

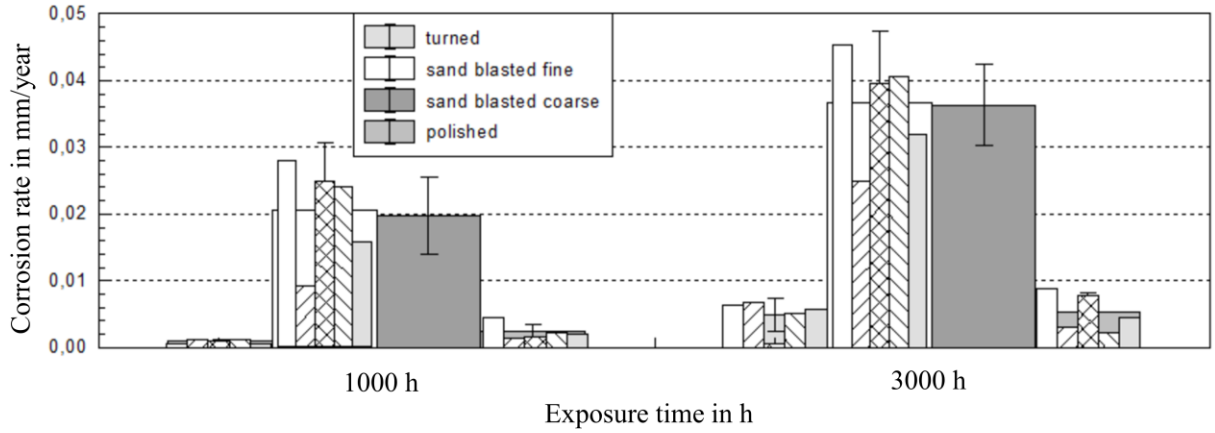

Figure 3: *Influence of surface treatment prior to exposure of 1.4542 to and CO_2 saturated saline aquifer water at 60 °C and ambient pressure on the corrosion behavior and different samples*

A corrosion rate of 0.005 mm/year was measured for technical and polished surfaces after 3000 h of exposure, whereas sand blasted samples revealed corrosion rates as high as 0.036 mm/year. Coupons with sand blasted surfaces give highest corrosion rates with no difference whether fine or coarse sand was used. Sand blasting possibly activates the steel surface damaging the passivating layer and leaving a larger surface area exposed to the corrosive environment. There are two possible explanations: First, larger activated surface areas enable diffusion reactions along the entire surface (not only locally) that result in higher corrosion rates and further metal deterioration. Second, internal parameters of the crystal lattice are changed by sand blasting causing a more reactive surface, subsequently decreasing the corrosion resistance (Ahmed et al., 2015). Also compressive stress resulting from sand blasting may influence the corrosion behaviour more negatively than high surface roughness (Aparicio, Gil, Fonseca, Barbosa, Planell, 2003). Irrespectively of tensile or compressive stress Lv et al., 2016 state that strain induces fast reaction of the metal surface promoting its dissolution in corrosive environment. This agrees with Zhang et al., 2016 correlating the micro crack density on the metal surface with residual stress indicating that residual stress enhances micro cracking. Engineering a CCS-site or geothermal power plant this study shows that technical surfaces offer sufficient corrosion resistance for static components.

3.2 Influence of Surface Condition on Corrosion Fatigue Behaviour

For the steel quality 1.4043 (X46Cr13) no significant dependence of the surface roughness on the fatigue behavior after fine machining was detected. Surface roughness of as-machined fatigue specimens varied between 3.6 and 4.7 µm and 30 specimen were analyzed. This particular steel quality does not show good corrosion resistance in CCS-environment. Therefore it may be assumed that corrosive attack completely outweighs the surface influence.

For the steel quality DSS 1.4462 (X2CrNiMoN22-5-3) generally the endurance limit for specimen of cycled in air is higher by a factor of 2.5 (Figure 4) compared to specimen cycled in saline aquifer water. The endurance limit of polished duplex stainless steel X2CrNiMoN22-5-3 in air is approximately 485 MPa with regard to a fatigue limit of 10^7 cycles (P_f = 50%, purely alternating push/pull load). The corrosion fatigue behavior of this steel in geothermal environment of the Northern German Basin resulted in a maximum cycle number of 4.2×10^6 at 290 MPa load amplitude using an electrically uninsulated experimental setup (Wolf et al., 2016). Results were obtained by means of linear regression (Equation 2):

$$N_{50} = N_A \cdot \left(\frac{S_a}{S_A}\right)^{-k} \quad for\ S_a \geq S_A \tag{2}$$

with:

- N_{50}–50 % probability cycle value
- N_A–reference cycle value
- S_A–reference stress value
- S_a–selected stress value

The characteristic gradient of the uninsulated curve of specimens with technical surfaces exhibits a slope coefficient k = 8.78 common for corrosion fatigue behavior of steels. The slope coefficient is higher by a factor of 2 for polished surfaces: k = 9.006). The scatter range TN describes the very low cycle probability scattering between 10% and 90% at 1:1.35 (Equation 3) indicating identical failure mechanisms for this specific set of specimens. For polished surfaces the scatter range is even higher: 1:1.9464, possibly due to a smaller number of specimens tested. For a small number of experiments the scatter range increases because exceptional tests results significantly influence the overall test tendency. In general, increasing the number of test results will lead to a significant change in the scatter range and slope coefficient.

$$T_N = 1 : \frac{\log N_{90}}{\log N_{10}} \tag{3}$$

If the cycles to failure are not only compared within one set of surface treatment, a significant difference is demonstrated comparing polished to technical specimen surfaces. The

line of regression of specimens with technical surfaces has greater negative slope (steeper) (k=8.78) than that of specimen with polished surfaces (k=19.006). Comparing slope coefficients k reveals that lines of regression with small number of k decline greater than those with large numbers of k.

The corrosive environment of the Northern German Basin presupposes that specimen with technical surfaces (average surface roughness 3.2 µm) perform better at stress amplitudes higher than 270 MPa than polished (average surface roughness 1.59 µm). At stress amplitudes S_a below 270 MPa polished surfaces reveal much higher numbers of cycles to failure. For example at S_a=300 MPa P50% (50% probability of survival) of specimen with technical surfaces is: $5x10^5$ cycles to failure whereas for specimen with polished surfaces P50% is only $1.5x10^5$ cycles to failure. On the other hand at S_a=250 MPa P50% (50% probability of survival) of specimen with technical surfaces is: $1.5x10^6$ cycles to failure whereas for specimen with polished surfaces P50% is $4x10^6$ cycles to failure.

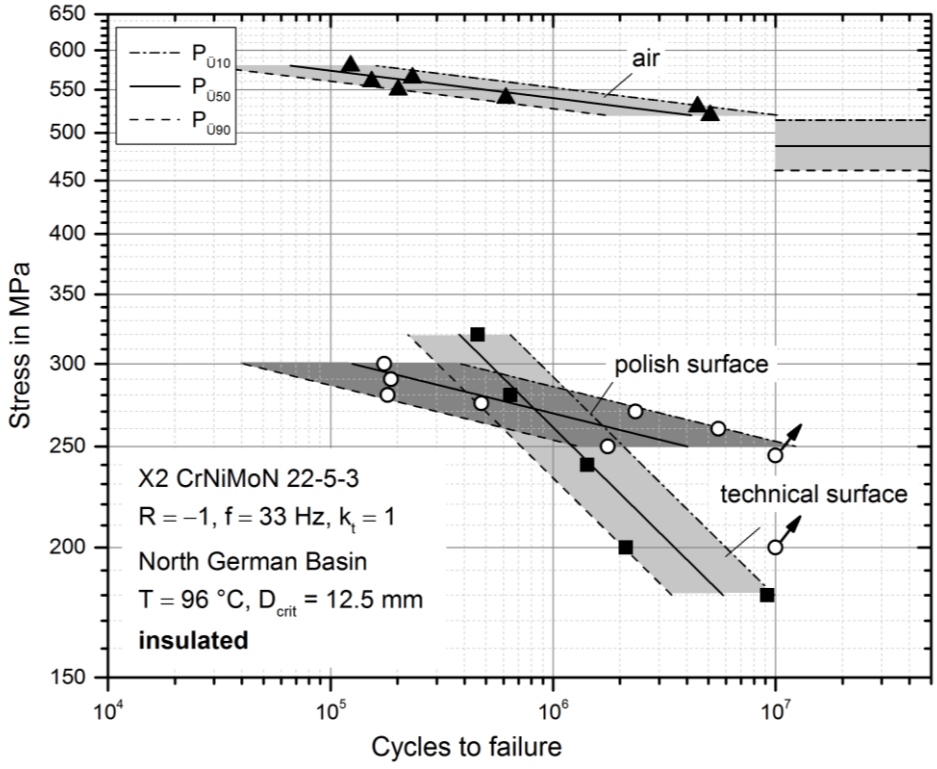

Figure 4: *S-N curve of 1.4462 X2CrNiMoN22-5-3 in air and in corrosive media Northern German Basin at 98 °C after machine turning (technical surface) and polishing (polished surface)*

Approach via Residual Stress: Sanjuro et al., 2010 proved that the surface finishing accompanied with the removal of surface stress raisers contributes mostly to the enhanced

corrosion fatigue behavior. Residual stress, however, only accounts for 10%. Still, one possible explanation of this surface dependent fatigue behavior is that at stress amplitudes above 275 MPa the surfaces of turned specimen (technical surface) underwent microstructural hardening processes during machining due to plastic deformation (Figure 5) resulting in residual stress. The procedure of turning implements compressive stress surpassing the increased surface roughness of this finishing process. Therefore, at stress amplitudes above 275 MPa residual stress results in enhanced corrosion fatigue behaviour. At 275 MPa the regression lines overlap indicating that at 275 MPa stress amplitude the surface condition has nearly no influence on the corrosion fatigue behavior. At stress amplitudes below 275 MPa the number of cycles to failure decreases as a function of increasing surface roughness. Residual stress is outweighed by corrosion reactions due to greater surface roughness at low stress amplitudes. At the same time the difference in number of cycles to failure for polished and technical surfaces increases with deceasing stress amplitudes indicating that the surface roughness can be neglected for small stress amplitudes. However, at increasing stress amplitudes the surface roughness of engineering materials in geothermal and CCS environment should be kept as small as technically and economically possible.

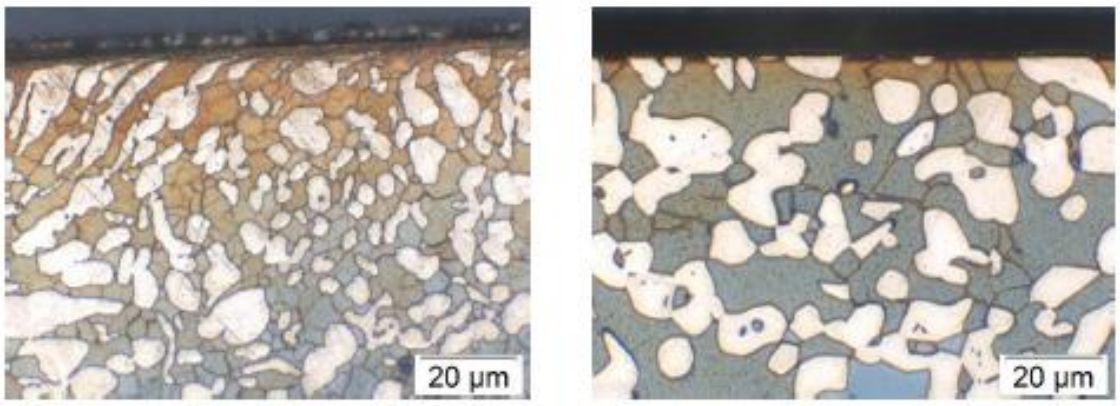

Figure 5: *Microstructure of 1.4462 X2CrNiMoN22-5-3 after Machine Turning (left) and polishing (right)*

Approach via Crack Growth: The microstructure and crack propagation have been described by Wolf et al., 2016. Failure cause is corrosion fatigue in the passive state due to the PREN and high chromium content. However, there is no evidence on the whether mechanical stress or corrosion pits act as crack initiation.

The fatigue cracks perpendicular to the layered duplex structure proceed alpha and gamma phase of the alloy likewise without a preferred propagation phase. Major and secondary

cracks are predominantly perpendicular to the direction of applied load. The major cracks finally leading to failure show clear residual opening with macro dimensions predominantly occurring close to the specimen's critical cross-section (Wolf et al., 2016). Secondary micro dimensional fatigue cracks do not possess measurable residual openings. Towards its ending the crack moderately branches out and follows partially curved pathways. Still, there is no evidence on the dependence of the surface condition that may be concluded from the crack pathway or the microstructure at the crack region.

However, another possible explanation is that the reason for supercritical crack growth changes after exceeding stress amplitudes above 275 MPa. However, as stated before, the mechanism of failure will remain the same for both cases indicated by the scatter ranges of both individual test series. However, at stress amplitudes greater 275 MPa the push-pull load leads to overall tensile stress in the specimen surface resulting in micro cracks (Figure 6). Further cycles alternately open and close the crack exposing the crack flanks to the highly corrosive brine. Due to a low solubility limit in aqueous solutions (pKsp = 10.54 at 25 ◦C (Banaś et al., 2007; Pfennig and Kranzmann, 2012; Lopez, Perez and Simison, 2003) siderite forms as a result from the transient phase precipitation of $Fe(OH)_2$ (Pfennig and Kranzmann, 2012; Pfennig et al., 2017) and segregate. Further mechanical stress and the strain mismatch of corrosion layer and base metal cause crack growth until failure. Because in general, higher strength results in higher endurance limits, the higher surface strength due to compressive stress resulting from the machining process results in a higher number of cycles to fatigue for technical surfaces.

Below 275 MPa the crack growth is not initiated by micro cracks but via pit corrosion on the surface layers –the mechanism was described above. These will inevitably lead to crack growth and further crack propagation (Figure 6) resulting in early failure. Wolf at al., 2016 described that the CCS environment of the Northern German Basin may lead to intergranular corrosion preferably of the austenitic phase in duplex stainless steel 1.4462. Pit cavities are associated with a secondary crack and material deterioration in the boundary region of crack and pit. Initial pits grow and after proceeding a critical size the notch effect results in fatigue crack formation. Therefore it is very likely that corrosion prior to micro cracking is primarily cause for fatigue failure under given experimental conditions. Because here pitting is reason for crack initiation and not micro cracks, a polished surface is preferable because it provides better resistance to corrosive attack and higher numbers of cycles to failure. Therefore at low stress

pitting is the initiating process whereas at high stress amplitudes the formation of micro cracks is reason for crack initiation, growth and failure.

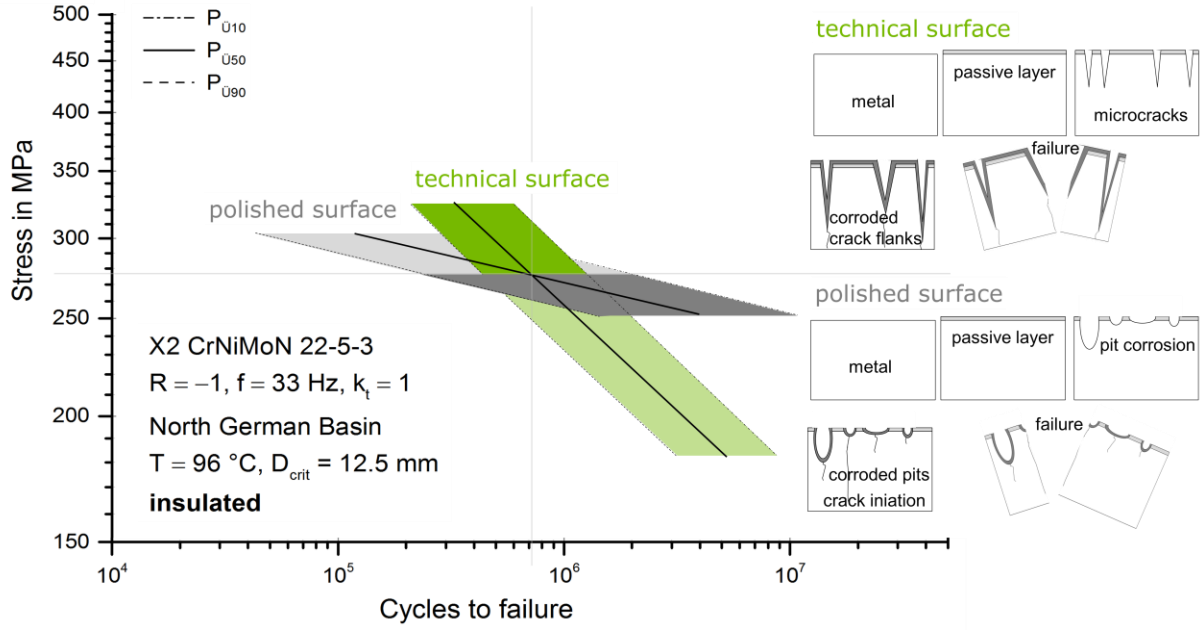

Figure 6: *S-N curve of 1.4462 X2CrNiMoN22-5-3 in air and in corrosive media Northern German Basin at 98 °C after machine turning (technical surface) and polishing (polished surface)*

Corrosion fatigue results agree well with results from static exposure tests with smooth surfaces giving best results for static exposure and dynamic exposure with high load. However, high surface roughness with no overlying mechanical stress leads to good corrosion resistance. Because for components facing corrosion fatigue the corrosion initiation will inevitably lead to components failure and therefore reduce the number of cycles to failure. At low stress amplitudes or static load both, corrosion resistance and high numbers of cycles to failure, will be achieved with technical surfaces rather than with polished surfaces. These results still have to be verified, but there is no obvious dependence on the mechanism of failure. Deriving from the coefficient of slopes and scatter range the failure mechanisms are similar in each test series.

4. Conclusion

Martensitic stainless steel X5CrNiCuNb16-4 (1.4542, AISI 630) with different surface conditions was exposed up to 1/2 year (3000 h) to CO_2-saturated saline aquifer water similar to the conditions in the Stuttgart Aquifer at ambient pressure and 60 °C in laboratory experiments. Additionally, corrosion fatigue experiments (ambient pressure, technically clean CO_2, saline aquifer water of the Northern German Basin) were performed using specimen of X46Cr13

(1.4043, AISI 420C) with regard to the influence of the roughness of technical surfaces on the number of cycles to failure at different stress amplitudes. Specimen of DSS X2CrNiMoN22-3-2 (1.4462) with different surfaces (technical surfaces after machining and polished surfaces) were tested at 98 °C between 175 MPa and 325 MPa (load amplitude) in artificial brine (Northern German Basin).

$FeCO_3$ and FeOOH precipitate not depending on the original surface roughness. Corrosion rates for polished and technical surfaces were below 0.005 mm/year in CO_2-saturated saline aquifer brine while sand blasting lead to corrosion rates higher by a factor of 7 (0.035 mm/year). Possibly this is due to micro cracking induced residual surface stress and fast corrosion within crack flanks especially on sand blasted specimen.

In general technical surfaces are giving good corrosion resistance for static corrosion and sufficiently high numbers of cycles to failure regarding corrosion fatigue in the active or passive state at low stress amplitudes in CCS and geothermal environment. The surface roughness (Rz=2.6–4.6) does not influence the corrosion fatigue behavior within one set of experiments, but different surface roughness after different surface treatments (Rz=~3.2 for turned surfaces and Rz=~1.59 for polished surfaces) have large impact. For duplex stainless steel 1.4462 the equilibrium at 98 °C in the saline water of the Northern German Basin was 275 MPa. At high stress amplitudes technical surfaces are preferred to achieve high numbers of cycles to failure. Technical surfaces tested at stress amplitudes above 275 MPa (P50% at Sa 300 MPa=$5x10^5$) endured more cycles to failure than polished surfaces (P50% at Sa 300 MPa=$1.5x10^5$). Rather low scatter ranges (technical surface: TN=1:1.35, polished surface: TN=1.1.95) indicate no change in failure mechanism. At low stress pitting is likely to be the initial crack growth process whereas at high stress amplitudes the formation of micro cracks is reason for crack propagation and failure.

Results from static and dynamic tests are in very good agreement. With no regard to the corrosion mechanism at low stress amplitudes or static load both, good corrosion resistance and sufficient numbers of cycles to failure will be achieved with technical surfaces in CCS environment. Also at very high stress amplitudes technical surfaces perform satisfyingly possibly due to residual stress from surface machining. It may be assumed that this residual stress enhances fatigue behavior outweighing corrosive attack even of surfaces with high surface roughness.

5. Acknowledgements

This work was supported by the FNK (Fachkonferenz für wissenschaftlichliche Nachwuchskräfte) of the Applied University of Berlin, HTW and by IMPACT (EU-Project EFRE 20072013 2/21). The authors would like to thank Andre Gröber, Rainer Wiegand, Roman Simkin and Roman Afanasiev for their worthy contribution to this paper.

References

Abdulstaar M., Mhaede M., Wollmann M., Wagner L. (2014). Investigating the effects of bulk and surface severe plastic deformation on the fatigue, corrosion behaviour and corrosion fatigue of AA5083. Surface & Coatings Technology, 254, 244–251. https://doi.org/10.1016/j.surfcoat.2014.06.026

Ahmed A. A., Mhaede M., Basha M., Wollmann M., Wagner L. (2015). The effect of shot peening parameters and hydroxyapatite coating on surface properties and corrosion behavior of medical grade AISI 316L stainless steel. Surface & Coatings Technology, 280, 347–358. https://doi.org/10.1016/j.surfcoat.2015.09.026

Akbari Mousavi S.A.A., Sufizadeh A.R. (2009). Metallurgical investigations of pulsed Nd:YAG laser welding of AISI 321 and AISI 630 stainless steels. Materials & Design 30, (8), 3150-3157. https://doi.org/10.1016/j.matdes.2008.11.026

Alvarez-Armas I. (2008). Duplex Stainless Steels: Brief History and Some Recent Alloys. Recent Patents on Mechanical Engineering, 1 (1), 51–57 https://doi.org/10.2174/2212797610801010051

Aparicio C., Gil F.J., Fonseca C., Barbosa M., Planell J.A. (2003). Corrosion behaviour of commercially pure titanium shot blasted with different materials and sizes of shot particles for dental implant applications. Biomaterials, 24, 263. https://doi.org/10.1016/S0142-9612(02)00314-9

Arnold N., Gümpel P., Heitz T.W. (1999). Chloride induced corrosion on stainless steels at indoor swimming pools atmospheres Part 2: influence of hypochlorite. Materials and Corrosion, 49, 140–145. https://doi.org/10.1002/(SICI)1521-4176(199903)50:3<140::AID-MACO140>3.0.CO;2-3

Banaś, J., Lelek-Borkowska, U., Mazurkiewicz B., Solarski W. (2007). Effect of CO2 and H2S on the composition and stability of passive film on iron alloy in geothermal water. Electrochimica Acta, 52, 5704–5714. https://doi.org/10.1016/j.electacta.2007.01.086

Bäßler R., Sobetzki J., Klapper H.S. (2013). Corrosion Resistance of High-Alloyed Materials in Artificial Geothermal Fluids. Vol. NACE Inter Nr. Corrosion, Orlando, USA, paper 2327.

Beuth Verlag GmbH (2009). Korrosion der Metalle - Korrosionsuntersuchungen - Teil 1: Grundsätze DIN 50905-1:2009-09.

Buschermöhle H. (1996). Vereinheitlichung von Proben für Schwingungsversuche. FKM Forschungsheft 217.

Carvalho D.S, Joia C.J.B, Mattos O.R. (2005). Corrosion rate of iron and iron-chromium alloys in CO_2-medium. Corrosion Science, 47, 2974-2986. https://doi.org/10.1016/j.corsci.2005.05.052

Choi, Y.-S. and Nešić, S. (2008). Corrosion behaviour of carbon steel in supercritical CO2-water environments. No. 09256 NACE Corrosion Conf. & Expo, New Orleans, Louisiana, USA, March 16th – 20th.

Cui, Z.D., Wu, S.L., Zhu, S.L., Yang, X.J. (2006). Study on corrosion properties of pipelines in simulated produced water saturated with supercritical CO_2. Applied Surface Science, 252, 2368-2374. https://doi.org/10.1016/j.apsusc.2005.04.008

Engelmohr F. und Fiedler B. (1991). Erhohung der Dauerfestigkeit geschmiedeter Pleuel durch Kugelstrahlen unter Vorspannung. Mat.-wiss. u. Werkstofftech., 22, 211-216. https://doi.org/10.1002/mawe.19910220606

Evgenya B., Hughesa T., Eskinba D. (2016). Effect of surface roughness on corrosion behaviour of low carbon steelin inhibited 4 M hydrochloric acid under laminar and turbulent flow conditions. Corrosion Science, 103, 196–205. https://doi.org/10.1016/j.corsci.2015.11.019

Foct J., Akdut N. (1993). Cleavage-like fracture of austenite in duplex stainless steel. Scripta Metallurgica et Materialia, 29 (2), 153–158. https://doi.org/10.1016/0956-716X(93)90300-H

Förster, A et al. (2010) Reservoir characterization of a CO_2 storage aquifer: The Upper Triassic Stuttgart Formation in the Northeast German Basin. Mar. Pet. Geol., 27, 2156–2172. https://doi.org/10.1016/j.marpetgeo.2010.07.010

Förster, A., Norden, B. Zinck-Jørgensen, K. Frykman, P. Kulenkampff, J. Spangenberg, E. Erzinger, J. Zimmer, M. Kopp, J. Borm, G. Juhlin, C. Cosma, C. Hurter, S. (2006), Baseline characterization of the CO2SINK geological storage site at Ketzin, Germany:

Environmental Geosciences, 13 (3), 145-161. https://doi.org/10.1306/eg.02080605016

Gale, J. Davison J., (2004). Transmission of CO_2 – safety and economic considerations. Energy, 29, 1319–1328. https://doi.org/10.1016/j.energy.2004.03.090

Grümpel P. et al. (2008), Rostfreie Stähle: Grundwissen, Konstruktions- und Verarbeitungshinweise, 4. Völlig neu bearbeitete Auflage, Expert Verlag, Renningen. ISBN 978-3-8169-2689-4 (pg. 1-3,31-32,51,53-55,57,78).

Han J., Zhang J., Carey J.W. (2011). Effect of bicarbonate on corrosion of carbon steel in CO_2-saturated brines. Journal of Green House Gas Control, 5, 1680-1683. https://doi.org/10.1016/j.ijggc.2011.08.003

Islam A.W., Sun A.Y. (2016). Corrosion model of CO_2 injection based on non.isothermal wellbore hydraulics. International Journal of Greenhouse Gas Control, 54, 219-227. https://doi.org/10.1016/j.ijggc.2016.09.008

Kissinger A., Noack V., Knopf S., Scheer D., Konrad W., Class H. (2014). Characterization of reservoir conditions for CO_2 storage using a dimensionless Gravitational Number applied to the North German Basin. Sustainable Energy Technologies and Assessments, 7, 209–220. https://doi.org/10.1016/j.seta.2014.06.003

Kleemann U. und Zenner H. (2006). Structural component surface and fatigue strength – Investigations on the effect of the surface layer on the fatigue strength of structural steel components. Mat.-wiss. u. Werkstofftech., 37 (5) 349-373. https://doi.org/10.1002/mawe.200600995

Lee S. M., Lee W. G., Kim Y. H., Jang H. (2012). Surface roughness and the corrosion resistance of 21Cr ferritic stainless steel. Corrosion Science 63 404–409. https://doi.org/10.1016/j.corsci.2012.06.031

Llaneza V., Belzunce F.J. (2015). Study of the effects produced by shot peening on the surface of quenched and tempered steels: roughness, residual stresses and work. Applied Surface Science, 356, 475–485 https://doi.org/10.1016/j.apsusc.2015.08.110

Lo I.-H., Tsai W.-T (2007). Effect of selective dissolution on fatigue crack initiation in 2205 duplex stainless steel. Corrosion Science, 49 (4), 1847–1861. https://doi.org/10.1016/j.corsci.2006.10.013

Lopez D.A., Perez T., Simison S.N. (2003). The influence of microstructure and chemical composition of carbon and low alloy steel in CO_2 corrosion. A state of the art appraisal Materials and Design, 24, 561-575. https://doi.org/10.1016/S0261-3069(03)00158-4

Lv J., Guo W., Liang T. (2016). The effect of pre-deformation on corrosion resistance of the passive film formed on 2205 duplex stainless steel. Journal of Alloys and Compounds, 686, 176-183. https://doi.org/10.1016/j.jallcom.2016.06.003

Maranhão C., Davim J.P. (2010) Finite element modelling of machining of AISI 316steel: numerical simulation and experimental validation. Simul. Modell. Pract.Theory, 18, 139–156. https://doi.org/10.1016/j.simpat.2009.10.001

Martin M., Weber S., Izawa C., Wagner S., Pundt A., Theisen W. (2011). Influence of machining-induced martensite on hydrogen-assisted fracture of AISI type 304austenitic stainless steel. Int. J. Hydrogen Energy, 36, 11195–11206. https://doi.org/10.1016/j.ijhydene.2011.05.133

Mathis R. (1987). Initiation and early growth mechanisms of corrosion fatigue cracks in stainless steels. Journal of Materials Science, 22 (3), 907–914. https://doi.org/10.1007/BF01103528

Moreira R.M., Franco C.V., Joia C.J.B.M., Giordana S., Mattos O.R. (2004). The effects of temperature and hydrodynamics on the CO2 corrosion of 13Cr and 13Cr5Ni2Mo stainless steels in the presence of free acetic acid. Corrosion Science 46 (2004) 2987-3003. https://doi.org/10.1016/j.corsci.2004.05.020

Mu L.J., Zhao W.Z. (2010). Investigation on carbon dioxide corrosion behavior of HP13Cr110 stainless steel in simulated stratum water. Corrosion Science, 52, 82-89. https://doi.org/10.1016/j.corsci.2009.08.056

Nešić, S. (2007). Key issues related to modelling of internal corrosion of oil and gas pipelines – A review. Corrosion Science, 49, 4308–4338. https://doi.org/10.1016/j.corsci.2007.06.006

Nor Asma R.B.A., Yuli P.A., Mokhtar, C.I. (2010). Study on the effect of surface finish on corrosion of carbon steel in CO2environment. Journal of Applied Science, 11, 2053–2057.

Pfennig A., Heynert K., Wolf M., Böllinghaus T. (2014). First in-situ Electrochemical Measurement During Fatigue Testing of Injection Pipe Steels to Determine the Reliability of a Saline Aquifer Water CCS-site in the Northern German Basin. Energy Procedia, 63, 5773-5786. https://doi.org/10.1016/j.egypro.2014.11.610 https://doi.org/10.1016/j.egypro.2014.11.609

Pfennig A., Kranzmann A. (2012). Effect of CO2 and pressure on the stability of steels with different amounts of Chromium in saline water. Corrosion Science, 6, 441–452 https://doi.org/10.1016/j.corsci.2012.08.041

Pfennig A., Linke B., Kranzmann A. (2011). Corrosion behavior of pipe steels ex-posed for 2 years to CO2-saturated saline aquifer environment similar to the CCS-site Ketzin, Germany. Energy Procedia, 4, 5122-5129. https://doi.org/10.1016/j.egypro.2011.02.488

Pfennig A., Wolf M., Bork C.-P., Trenner S., Wiegand R (2014). Comparison between X5CrNiCuNb16-4 and X46Cr13 under Corrosion Fatigue. In: Corrosion 2014, San Antonio, Texas, USA, NACE International, Paper No. 3776.

Pfennig A., Wolf M., Gröber A., Böllinghaus T., Kranzmann A. (2016). Corrosion fatigue of 1.4542 exposed to a laboratory saline aquifer water CCS-environment, 13th International Conference on Greenhouse Gas Control Technologies, GHGT-13, 14th -18th November 2016, Lausanne, Switzerland.

Pfennig, A. Kranzmann A. (2011). Reliability of pipe steels with different amounts of C and Cr during onshore carbon dioxid injection. International Journal of Greenhouse Gas Control, 5, 757–769. https://doi.org/10.1016/j.ijggc.2011.03.006

Pfennig, A., Wolthusen, H., Kranzmann, A. (2017). Unusual corrosion behavior of 1.4542 exposed a laboratory saline aquifer water CCS-environment. Energy Procedia, 114, 5229-5240.
https://doi.org/10.1016/j.egypro.2017.03.1678 https://doi.org/10.1016/j.egypro.2017.03.1679

Pfennig, A., Wolthusen, H., Wolf, M., Kranzmann, A. (2014). Effect of heat treatment of injection pipe steels on the reliability of a saline aquifer water CCS-site in the Northern German Basin Energy Procedia, 63, 5762-5772.

Prosek T., Le Gac A., Thierry D., Le Manchet S., Lojewski C., Fanica A., Johansson E., Canderyd C., Dupoiron F., Snauwaert T., Maas F., Droesbeke B. (2014). Low temperature stress corrosion cracking of austenitic and duplex stainless steels under chloride deposits. Corrosion, 70 (10), 1052–1063. https://doi.org/10.5006/1242

Ruhl A.S., Goebel, A. Kranzmann, A. (2012). Corrosion Behavior of Various Steels for Compression, Transport and Injection for Carbon Capture and Storage. Energy Procedia, 23, 216-225 https://doi.org/10.1016/j.egypro.2012.06.074

Sanjurjo P., Rodríguez C., Pariente I. F., Belzunce F.J., Canteli A.F. (2010). The influence of

shot peening on the fatigue behaviour of duplex stainless steels. Procedia Engineering, 2, 1539-1546. https://doi.org/10.1016/j.proeng.2010.03.166

Schultze S., Göllner J., Eick K., Veit P., Heyse H. (2001). Selektive Korrosion von Duplexstahl. Teil 1: Aussagekraft herkömmlicher und neuartiger Methoden zur Untersuchung des Korrosionsverhaltens von Duplexstahl X2CrNiMoN22-5-3 unter besonderer Berücksichtigung der Mikrostruktur. Materials and Corrosion, 52 (1), 26–36. https://doi.org/10.1002/1521-4176(200101)52:1<26::AID-MACO26>3.0.CO;2-N https://doi.org/10.1002/maco.19500010108

Seiersten M. (2001), Material selection for separation, transportation and disposal of CO_2, Corrosion paper no. 01042.

Shahryari A., Kamal W., Omanovic S. (2008).The effect of surface roughness on the efficiency of the cyclic potentiodynamic passivation (CPP) method in the improvement of general and pitting corrosion resistance of 316LVM stainless steel. Materials Letters, 62, 3906–3909. https://doi.org/10.1016/j.matlet.2008.05.032

Takemoto M. (1984). Study on the failure threshold stress criteria for the prevention and mechanism of stress corrosion cracking, in: Faculty of Science and Engineering, Aoyama Gakuin University 6-16-1, Chitosedai, Setagayaku, Tokyo, 157 Japan, Int'l. Congress Metallic Corr.

Thomas D.C. (2005). Carbon Dioxide Capture for Storage in Deep Geologic Formations – Results from CO_2 Capture Project, Volume 1: Capture and Separation of Carbon Dioxide form Combustion Sources, CO_2 Capture Project, Elsevier Ltd UK, ISBN 0080445748.

Vollmar J. (1994). Schwingungsrisskorrosion des ferritisch-austenitischen Stahles X2CrNiMoN22-5-3 in 3 %iger NaCl-Lösung unter definierten Korrosions- und Wärmeübergangsbedingungen. Affirmed dissertation at the Kaiserslautern University. Kaiserslautern 3-6, pg. 46-51.

Wang J, Zou H. (2006). Relationship of microstructure transformation and hardening behavior of type 630 stainless steel. J Univ Sci Tech Beijing, 3, 213–221. https://doi.org/10.1016/S1005-8850(06)60045-5

Wei, L., Pang, X., Liu, C., Gao, K. (2015). Formation mechanism and protective property of corrosion product scale on X70 steel under supercritical CO_2 environment. Corrosion Science, 100, 404–420. https://doi.org/10.1016/j.corsci.2015.08.016

Wolf M., Afanasiev R., Böllinghaus T., Pfennig A. (2016). Investigation of Corrosion Fatigue of

Duplex Steel X2CrNiMoN22 5 3 Exposed to a Geothermal Environment under Different Electrochemical Conditions and Load Types, 13th International Conference on Greenhouse Gas Control Technologies, GHGT-13, 14th -18th November 2016, Lausanne, Switzerland.

Wu S.L, Cui Z.D., Zhao G.X., Yan M.L., Zhu S.L., Yang X.J. (2004). EIS study of the surface film on the surface of carbon steel form supercritical carbon dioxide corrosion. Applied Surface Science, 228, 17-25. https://doi.org/10.1016/j.apsusc.2003.12.025

Wu X.Q., Guan H., Han E. H., Ke W. and Katada Y. (2006). Influence of surface finish on fatigue cracking behavior of reactor pressure vessel steel in high temperature water. Materials and Corrosion 57, (11), 868-871. https://doi.org/10.1002/maco.200503963

Xu M., Zhangb Q., Yanga X.X., Wanga Z., Liub J., Li Z. (2016). Impact of surface roughness and humidity on X70 steel corrosion in supercritical CO_2 mixture with SO_2, H_2O, and O_2. Journal of Supercritical Fluids, 107, 286–297. https://doi.org/10.1016/j.supflu.2015.09.017

Zhang W., Fang K., Hu Y., Wang S., Wang X. (2016). Effect of machining-induced surface residual stress on initiation of stress corrosion cracking in 316 austenitic stainless steel. Corrosion Science, 108, 173–184. https://doi.org/10.1016/j.corsci.2016.03.008